# Grand Canonical Monte Carlo Simulation of Adsorption of Nitrogen and Oxygen in Realistic Nanoporous Carbon Models

**Amit Kumar, Raul F. Lobo, and Norman J. Wagner**
Center for Molecular and Engineering Thermodynamics, Dept. of Chemical Engineering, University of Delaware, Newark, DE 19716

*DOI 10.1002/aic.12356*
*Published online August 12, 2010 in Wiley Online Library (wileyonlinelibrary.com).*

*Adsorption of nitrogen and oxygen in nanoporous carbons (NPC) is simulated using grand canonical Monte Carlo simulations, where the Steele potential (developed for gas interactions with graphite) is used to represent gas–carbon interactions. NPC models used for the adsorption simulations are developed using an isothermal-isobaric (constant NpT) ensemble Monte Carlo algorithm whereby an initial polymer chain is evolved through a series of atomic displacement and bond rearrangement steps into the final carbon structure. These constant NpT carbon models are representative of real NPCs in terms of local structure and chemical composition. Predictions of nitrogen and oxygen sorption from our model NPCs show good agreement with experimental data. The isosteric heats of adsorption of both adsorbates lie within the range of experimental values for NPCs. Furthermore, the adsorption isotherms of the two gases showsemi-quantitative match with experimental adsorption isotherms.* © 2010 American Institute of Chemical Engineers *AIChE J,* 57: 1496–1505, 2011
*Keywords: adsorption/gas, membrane materials, nanotechnology, separation techniques, thermodynamics/statistical*

## Introduction

Amorphous carbons can be broadly classified into graphitizing and nongraphitizing carbons depending on whether they convert to graphite when treated at high temperatures.[1] Nanoporous carbon (NPC) is a type of nongraphitizing carbon prepared from the pyrolysis of carbon containing polymeric precursors, such as polyfurfuryl alcohol (PFA). NPCs have applications in a variety of fields such as gas purification[2] and catalysis.[3] Membranes prepared from NPCs have been shown to exhibit nitrogen-to-oxygen selectivity values as high as 30:1.[4] NPC is used extensively in the pressure swing adsorption process to separate nitrogen/oxygen and $CO_2$/hydrogen.[5] These materials have a narrow pore size distribution centered at approximately 5 Å.[2] The complicated pore structure of NPCs limits the applicability of traditional models (such as the Langmuir model) to experimental data to understand the adsorption thermodynamics.

Molecular simulation is increasingly being used to study gas adsorption in microporous materials[6–8] because, apart from generating the usual adsorption isotherms and heats of adsorption data, it allows one to view the process at an atomistic level and thus helps in the fundamental understanding of the process.

There have been several simulation studies involving adsorption of gas molecules and their mixtures in porous adsorbents such as zeolites,[6,9–13] carbon nanotubes,[7,14] activated carbons[8,15] and other materials.[16–20] Jiang et al.[21,22] have performed simulation studies of gas adsorption in NPCs using $C_{168}$ schwarzite (a hypothetical carbon structure with negative curvature[23]) as model NPC structure.

Correspondence concerning this article should be addressed to N. J. Wagner at wagnernj@UDel.Edu.

Adsorption characteristics of several carbonaceous materials (such as carbon nanotubes, $C_{60}$ fullerene, and $C_{168}$ schwarzite.) have also been compared using molecular simulation by Jiang et al.[24]

Various experimental studies of adsorption of gases (such as nitrogen and oxygen) in NPCs have been reported in literature.[25–27] The NPC samples most commonly used for gas adsorption studies are Takeda (3A and 5A) and Bergbau-Forschung. The equilibrium adsorptive capacities of the NPC samples for nitrogen and oxygen are quite similar. Thus, equilibrium separation of nitrogen-oxygen mixture is not possible by adsorption on NPCs. However, the uptake rate of oxygen in NPCs is higher than that of nitrogen, thus making the kinetic separation of these two gases possible over NPC beds.

Although nitrogen–oxygen separation using NPCs is a nonequilibrium (kinetic) phenomenon, a knowledge of the thermodynamics of gas adsorption in NPCs is still necessary. According to the solution-diffusion mechanism of gas transport in nanostructured materials, permeation is controlled by both diffusivity and solubility of the gas atoms/molecules in the membrane. The permeability is thus defined as the product of solubility and diffusivity of the adsorbed gas. Adsorption isotherms of gases can be used to obtain their solubility which, in conjunction with diffusivity data, can be used to calculate the permeability of the gases. Furthermore, adsorption isotherms are necessary for determining transport diffusivity using the Darken relation.[28]

To study adsorption in NPC using molecular simulation, a realistic atomistic model of an NPC is required. A novel Monte Carlo (MC) algorithm was developed by Kumar et al.[29] to generate realistic models of amorphous, microporous carbons. The algorithm, a constant NVT MC simulation method, generated carbon models whose properties compared favorably with those of real NPCs. However, real NPCs are prepared under conditions of constant pressure. Therefore, the MC algorithm has been modified to perform simulations at constant pressure, temperature, and system size, i.e., constant NpT. The NPC models generated using the constant NpT MC algorithm are used for adsorption simulations.

In this article, first the model structures obtained from this constant NpT MC algorithm are characterized and their structural properties compared with corresponding experimental results. Subsequently, the adsorption of nitrogen and oxygen in these NPC models is studied using grand canonical Monte Carlo (GCMC) simulations. The simulated adsorption results are compared with experimental adsorption data for these gases.

## Simulation Method

### *Generation of NPC models using constant NpT MC*

The constant NpT MC simulation method developed here to generate NPC models is similar to the constant NVT MC algorithm developed by Kumar et al.[29] The only difference between the two methods is that instead of a constant volume, the volume is allowed to vary to maintain a target system pressure. This is accomplished by a volume change move,[30,31] in addition to the displacement and bond rearrangement, MC moves used in the constant NVT algorithm. The volume change move can be implemented by changing the box volume, changing the box length,[32] or changing the logarithm of the box volume, ln $V$.[33] In the NPC generation algorithm, volume change moves are attempted by changing ln $V$. The extent of change in ln $V$ is chosen randomly but is constrained to be below a maximum value. Furthermore, this upper limit on the extent of change in ln $V$ is adjusted throughout the course of the simulation to obtain a 50% acceptance ratio for the volume change moves.

The algorithm can be broadly divided into the following three steps:

- Generate a starting carbon polymer representative of PFA.
- Carry out atomic displacement, bond rearrangement, and volume change moves on all the atoms of the system.
- Add hydrogen to the MC optimized structure and minimize energy.

The starting polymer is generated in exactly the same fashion as in the constant NVT method.[29] In every simulation, 4000 MC cycles are carried out on the starting carbon polymer. On an average, one MC cycle consists of 200 steps of atomic displacement moves, one step of bond rearrangement move, and two volume change moves. One step of any type is considered complete when all the atoms in the system have been displaced once. The atoms to be displaced in a step are chosen in random order, and no atom is displaced more than once in a step. The reader is referred to the article by Kumar et al.[29] for detailed definition of the bond rearrangement move. As the bulk of the simulation time is consumed by bond rearrangement moves, the constant NpT MC algorithm requires a similar computation time as the constant NVT MC algorithm, provided the system size is the same.

As in the constant NVT method, hydrogen is added (using Cerius$^2$ software[34]) to the structure obtained after 4000 MC cycles to satisfy the coordination requirements of the $sp^2$ carbons. Energy minimization is subsequently carried out on the structure to obtain the final NPC model.

To quantify the amount of free space in the different models, fractional free volumes of the NPC structures are calculated as follows: the simulation box is divided into a three-dimensional cubic mesh with adjacent node points 0.2 Å apart. A probe sphere is inserted at every node point, and the insertion is judged to be successful if there is no overlap between the probe and the carbon atoms, as defined by their Lennard-Jones (LJ) radii. The number of node points at which the insertion could be successfully carried out is divided by the total number of node points (or equivalently, insertion attempts) to obtain the fractional free volume.

The cavity size distribution (CSD) is the probability distribution of introducing a hard-sphere probe into the carbon structure without any overlaps between the probe and the carbon atoms. In this work, CSDs are calculated using the same approach as used in Ref. 29. A mesh size of 0.1 Å is used.

Bond anisotropy maps of the NPC models are generated to estimate the degree of anisotropy as quantified by the net orientation of C—C bonds. The maps for the structures are generated according to the method described in Ref. 29. To further quantify the level of anisotropy in the models, standard deviation of the bond anisotropy data is calculated. During the generation of anisotropy maps, the bond anisotropy data is calculated in the form of bond area density as a function of spherical angles $\theta$ and $\phi$, i.e., $\rho(\theta,\phi)$. So, the standard deviation of $\rho(\theta,\phi)$ is calculated using

**Table 1. Site–Site Lennard Jones Potential Parameters for Nitrogen and Oxygen Used in the GCMC Simulations**

| | C—N | C—O | N—N | O—O |
|---|---|---|---|---|
| $\sigma$ (Å) | 3.36 | 3.19 | 3.32 | 2.99 |
| $\varepsilon k_B$ (K) | 33.4 | 37.6 | 36.4 | 52.0 |
| $l$ (Å) | | | 1.10 | 1.208 |

Nitrogen and oxygen bond lengths ($l$) are also listed. $k_B$ is the Boltzmann constant.

$$\sigma_\rho = \frac{\sum_\theta \sum_\phi (\rho(\theta,\phi) - \bar{\rho})^2}{N-1} \tag{1}$$

where $\sum_\theta$ and $\sum_\phi$ represent sum over $\theta$ and $\phi$ respectively, $\bar{\rho}$ is the bond area density averaged over $\theta$ and $\phi$, and $N$ is the number of data points at which $\rho(\theta,\phi)$ is calculated. The ratio of the standard deviation and the average of bond anisotropy data, $\alpha = \sigma_\rho/\bar{\rho}$, is used as a quantitative measure of the level of anisotropy in the carbon structures. The higher the value of $\alpha$, the more anisotropic the structure would be.

### *Gas adsorption in NPC models*

GCMC simulations are used to simulate the adsorption of oxygen and nitrogen on model NPC structures. The NPC models used for the adsorption studies are obtained using the constant NpT MC algorithm described in the previous section. The adsorbate (nitrogen and oxygen) molecules are represented as two-site diatomic molecules. The site–site interactions amongst the adsorbates and between the adsorbates and NPC are modeled by the LJ potential.

LJ parameters and bond lengths used for nitrogen and oxygen molecules are listed in Table 1. The well-studied Steele potential[35] was used to model the interaction between the carbon atoms and the adsorbate molecules ($N_2$ and $O_2$). The interaction parameters for this potential are also listed in Table 1. A cutoff distance of $4\sigma_{C-N}$ in the case of nitrogen adsorption and $4\sigma_{C-O}$ in the case of oxygen adsorption is used for the LJ interactions. If $4\sigma_{C-N}$ or $4\sigma_{C-O}$ is larger than half the simulation box length, $L_{box}/2$ is used as the cutoff distance where $L_{box}$ is the simulation box dimension.

Lorentz-Berthelot mixing rules are used to calculate LJ interactions between the adsorbates and hydrogen atoms in the NPC.

Simulations are carried out to study single component adsorption of $N_2$ and $O_2$ in NPC models. The usual displacement, rotation, and insertion/deletion MC moves[31] are used, 20% of the moves are molecular displacement, 20% are molecular rotation, and the remaining 60% are insertion/deletion moves (insertion and deletion moves are assigned equal probability).

The isosteric heat of adsorption, $q_{st}$, is the differential heat released when an infinitesimal amount is transferred from the bulk phase to the adsorbed phase at constant temperature and pressure. As the partial molar volume of the adsorbate phase is usually negligible in comparison with that of the bulk phase, the isosteric heat of adsorption for single component adsorption can be expressed as[36]

$$q_{st} = -\left(\bar{H}^{b,*} - \bar{H}^b\right) + RT - \left(\frac{\partial U^a}{\partial N^a}\right)_T \tag{2}$$

**Table 2. List of NpT MC Simulations Performed Along with the Conditions at Which They Are Carried Out**

| Simulation No. | Starting Structure | Density (g/cm$^3$) | Corrected Skeletal Density (g/cm$^3$) |
|---|---|---|---|
| 1 | Polymer A | 1.23 | 1.47 |
| 2 | Polymer B | 1.27 | 1.52 |
| 3 | Polymer A[1] | 1.19 | 1.48 |

Polymers A and B are created from two different configurations of the lattice polymer backbone. Superscript in Simulation 3 denotes that the random number generation sequence for the Monte Carlo moves is different from that in Simulation 1. Density of the starting polymer in all the cases is 1.72 g/cm$^3$.

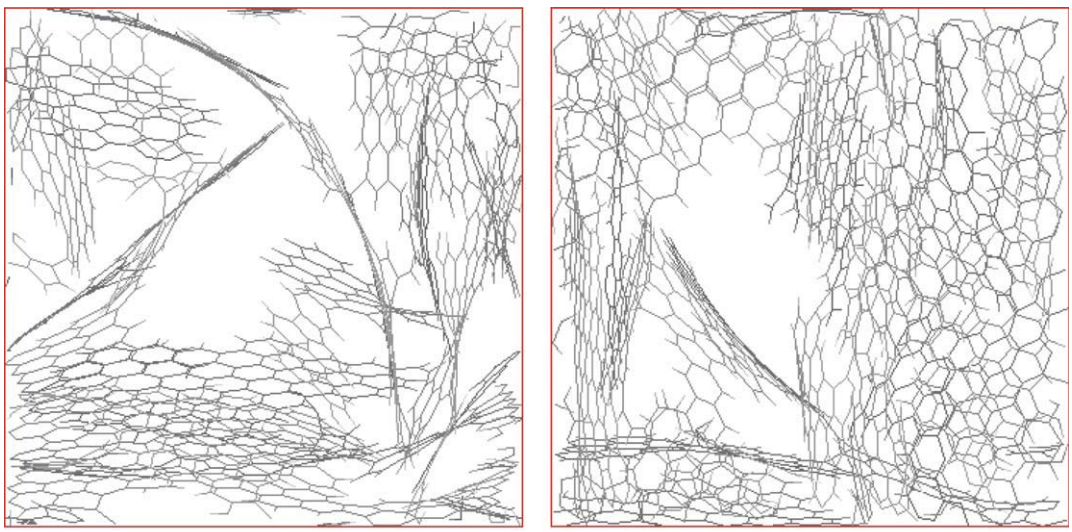


**Figure 1. Wire frame view of model NPC structures generated at conditions of (a) Simulation 2, and (b) Simulation 3 in Table 2.**

[Color figure can be viewed in the online issue, which is available at wileyonlinelibrary.com.]

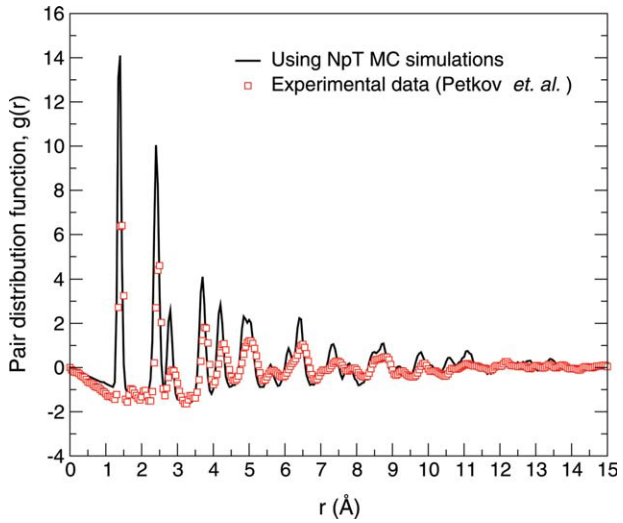


**Figure 2. PDF of model NPC structure obtained from Simulation 1.**

The experimental PDF (by Petkov et al.[37]) is also shown for comparison. [Color figure can be viewed in the online issue, which is available at wileyonlinelibrary.com.]

where $\left(\bar{H}^{b,*} - \bar{H}^{b}\right)$ is the departure function for the partial molar enthalpy in the bulk phase, $R$ is the universal gas constant, $U^a$ is the total adsorbate-adsorbent and adsorbate-adsorbate interaction energy, and $N^a$ is the number of adsorbate molecules. Assuming ideal gas behavior in the bulk phase, Eq. 2 becomes

$$q_{\mathrm{st}} = RT - \left(\frac{\partial U^a}{\partial N^a}\right)_T \tag{3}$$

The partial derivative $(\partial U^a/\partial N^a)_T$ can be obtained using fluctuation theory as

$$\left(\frac{\partial U^a}{\partial N^a}\right)_T = \frac{f(U^a, N^a)}{f(N^a, N^a)} \tag{4}$$

where $f(A,B) = \langle AB\rangle - \langle A\rangle\ \langle B\rangle$ and $\langle\ldots\rangle$ denotes ensemble average value.

The ideal gas equation is used to relate the chemical potential and the bulk pressure of the adsorbates in simulations carried out at low- to-moderate pressures. At high pressures, the Peng-Robinson equation of state (PREOS) is used.

In every GCMC simulation, a total of $2.5 \times 10^7$ MC moves are carried out. The system is equilibrated during the first $1.25 \times 10^7$ moves and data are collected during the rest of the simulation.

**Table 3. Fractions of 5-, 6- and 7-Membered Rings in the Final Structures Generated at Different Conditions (Outlined in Table 2)**

| Simulation No. | Percent of 5-Member Rings | Percent of 6-Member Rings | Percent of 7-Member Rings | Total Number of Rings |
|---|---|---|---|---|
| 1 | 5.7 | 91.2 | 3.1 | 421 |
| 2 | 6.7 | 88.7 | 4.6 | 435 |
| 3 | 4.7 | 92.2 | 3.1 | 421 |

**Table 4. Fraction of Carbon Atoms Having Different Number of Carbon Atom Neighbors in the Final Structures Generated at Different Conditions (Outlined in Table 2)**

| Simulation No. | Percent of C Atoms with 1 Neighbor | Percent of C Atoms with 2 Neighbors | Percent of C Atoms with 3 Neighbors |
|---|---|---|---|
| 1 | 0.5 | 28.0 | 71.5 |
| 2 | 0.3 | 28.7 | 71.0 |
| 3 | 0.5 | 29.8 | 69.7 |

## Results and Discussions

### *Properties of NPC models*

Three simulations are carried out changing the starting polymer configuration and random number generation sequence (for the MC moves), but holding the system parameters such as temperature and pressure fixed (at 800°C and 1 bar, respectively). The conditions at which these simulations are carried out are listed in Table 2. The starting structure for these simulations is set at a density of 1.72 g/cm$^3$, which is the experimental value reported by Petkov et al.[37] for NPCs prepared at 800°C. The NpT simulations lead to a reduction in density for all the cases considered, resulting in high free volumes in the NPC models. Figure 1 illustrates two model NPC structures obtained by constant NpT MC simulations corresponding to Simulation 2 and 3 (see Table 2). Both these structures show the presence of "holes" that extend across the length of the simulation box

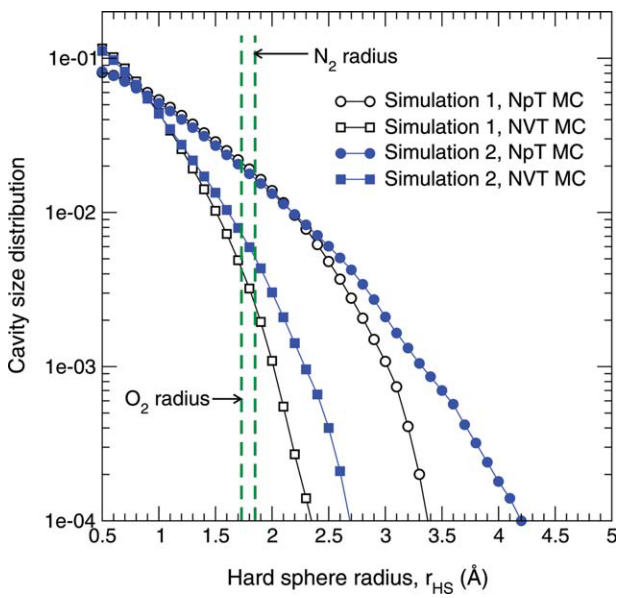


**Figure 3. CSDs of the NPC models generated from two different starting polymer conformations (simulations 1 and 2 in Table 2).**

CSDs of the corresponding NPCs generated using constant NVT MC simulations are also shown. The Lennard-Jones (LJ) radii of nitrogen and oxygen are represented as dashed vertical lines. [Color figure can be viewed in the online issue, which is available at wileyonlinelibrary.com.]

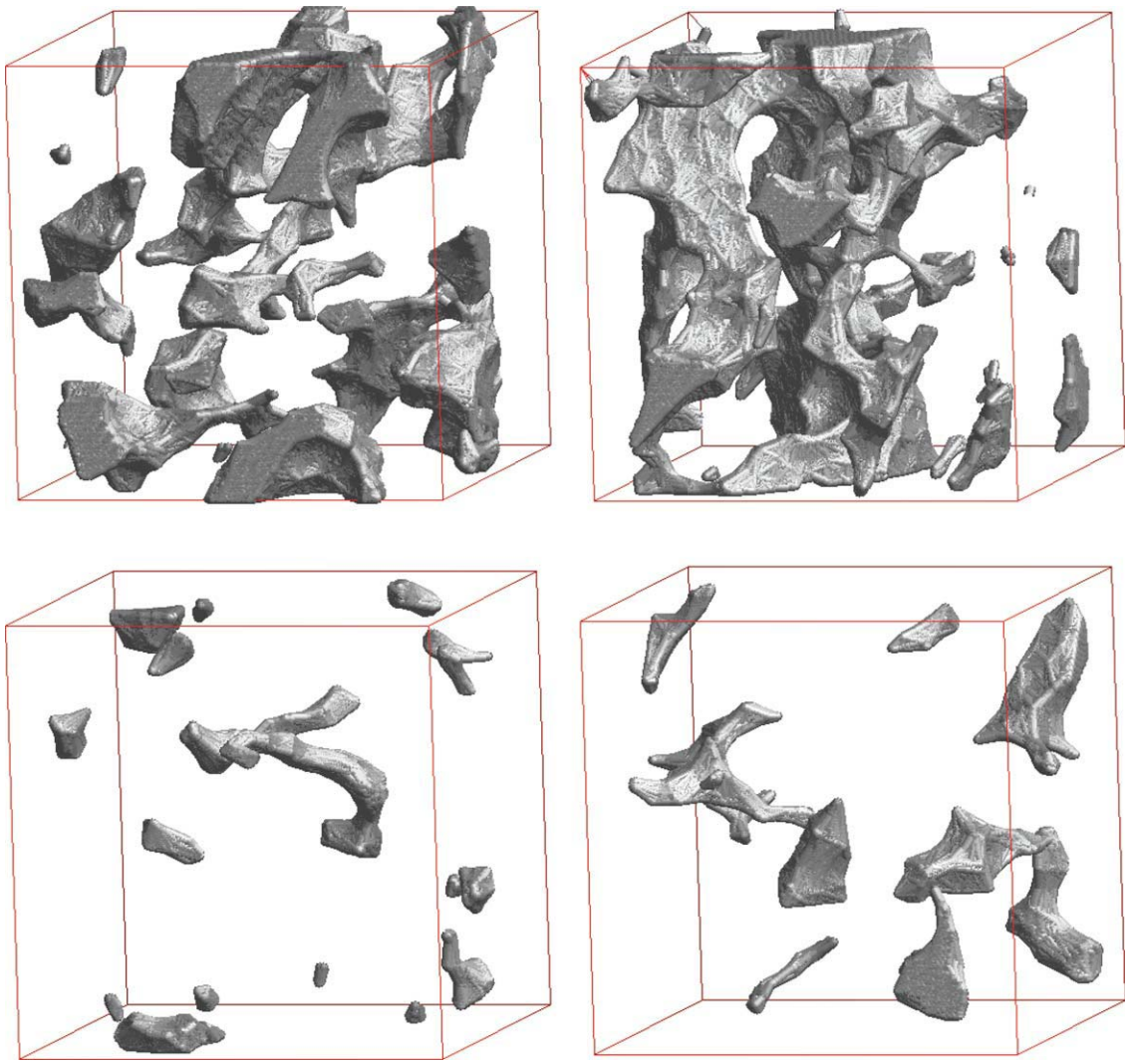

**Figure 4. Free volume maps obtained using hard sphere representation of nitrogen and oxygen molecules as probes are shown for NPC models generated under the conditions of Simulations 1 and 2 (see Table 2).**

The free volume maps for corresponding constant NVT carbon models have also been shown for comparison. [Color figure can be viewed in the online issue, which is available at wileyonlinelibrary.com.]

and can act as percolation pathways for gas transport. Thus, constant NpT MC simulations lead to an inhomogeneous carbon structure with significant "holes"

The volume used to calculate the density includes the void space in the models, thus giving values lower than what the actual skeletal density might be. Helium pycnometry is the most commonly used experimental technique to calculate skeletal densities. In this technique, the volume of pores or cavities in the material accessible by helium is excluded from the sample volume used to calculate the density. As a crude approximation to this method, corrected densities of the carbon models are calculated by subtracting the helium free volume of the structure from the simulation box volume and using this value to divide the total mass of the atoms in the box. The helium free volume of the structure is calculated using the approach outlined in the Section "Simulation Method". The corrected densities are listed in the last column of Table 2. All three NPC models have a corrected density of $\sim$1.5 g/cm$^3$. This value is somewhat lower than the experimental range of densities (1.6–1.72 g/cm$^3$[34,37] for industrially relevant NPCs and is caused by large expansion of the simulation box owing to the relatively low pressure of simulation.

The pair distribution function (PDF) of a sample NPC structure generated at the conditions of Simulation 1 is

**Table 5. Fractional Free Volumes of Different Carbon Models Obtained Using Nitrogen and Oxygen as Probe Molecules**

| | Percentage Free Volume | |
|---|---|---|
| Simulation No. | Using Nitrogen | Using Oxygen |
| 1 | 6.0 | 7.6 |
| 2 | 6.7 | 8.2 |
| 3 | 9.6 | 11.3 |

The carbon models are represented by their simulation numbers in Table 2.

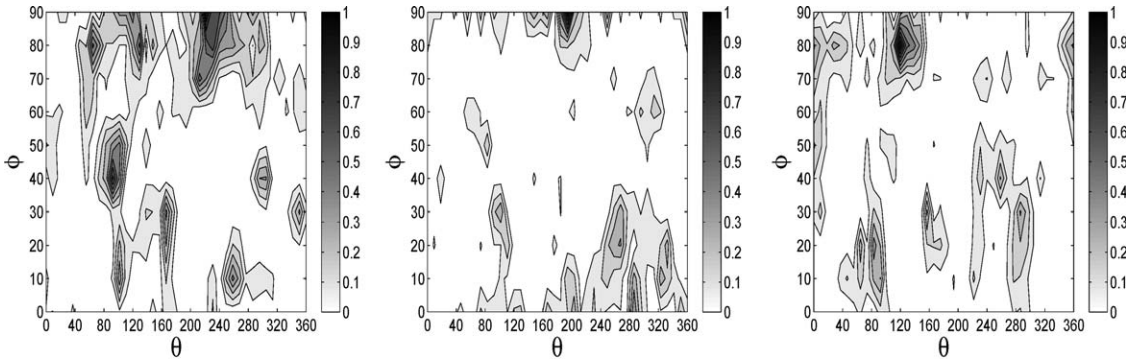


**Figure 5. Effect of change in starting polymer and random number generation sequence on the bond anisotropy maps of the constant NpT carbon models.**

Bond anisotropy maps are shown for NPC models generated by (a) Simulation 1, (b) Simulation 2, and (c) Simulation 3 (see Table 2). The highest value on the scale bars (i.e., 1) represents the maximum bond density (bonds per unit area) in the structure.

shown in Figure 2. PDFs of other structures used in this work correspond closely to the PDF in Figure 2 and hence have not been shown. Experimental PDF (by Petkov et al.[37]) of an NPC sample prepared at 800°C is also plotted in Figure 2. The simulated PDF shows good agreement with the experimental PDF in terms of the peak positions and the extent of correlation in the structure. This suggests the dense regions are representative of experimental NPCs.

NPC models generated from Simulations 1–3 (see Table 2) are used to study how changing simulation parameters, such as the configuration of the starting polymer or the random number generation sequence for the MC moves, affects the properties of the resulting NPC structure. Table 3 lists the fractions of 5-, 6- and 7-membered rings in different NPC models. The fractions of these rings do not vary appreciably with a change in either the starting polymer configuration or the random number generation sequence. The fraction of hexagonal rings, in all cases, is close to 90%. The total number of rings, which is a measure of the degree of $sp^2$ hybridization of the carbons, is nearly the same for these cases. In Table 4, the fraction of carbon atoms having 1, 2, and 3 carbon atom neighbors are listed for all the different NPC models. The fraction of carbons having three carbon atom neighbors is on average ~70%. Note that higher fraction of such three-coordinated carbons implies lower hydrogen-to-carbon ratio in the system. Consequently, all final structures have similar composition.

Figure 3 shows the CSDs of the NPC structures generated under the conditions of simulations 1 and 2 in Table 2. The CSDs show similar $N_2$ and $O_2$ insertion probabilities in both structures. Although both structures show the presence of cavities larger than 3 Å (in radius), the structure generated using polymer B has larger cavities than that generated from polymer A. For comparison, the CSDs of NPCs generated using the constant NVT MC method (as described in Ref. 29) are also plotted in Figure 3. These constant NVT structures were generated at the same conditions of temperature, box size, and starting structure as the two constant NpT structures. Upon inspection, it is evident that the constant NpT carbon structures exhibit significantly higher $N_2$ and $O_2$ insertion probabilities and have considerably larger cavities.

The free volume maps (using nitrogen as probe molecule) for structures obtained from Simulations 1 and 2 are shown in Figure 4. The structure from Simulation 2 shows larger free volume than the other structure and has "channels" extending across the length of the simulation box. Free volume maps of the corresponding structures generated using constant NVT MC method are also shown for comparison. The constant NpT NPCs have a much higher free volume than their constant NVT counterparts.

Fractional free volumes of the carbon models have been calculated using nitrogen and oxygen as probe molecules and are listed in Table 5. Carbon model corresponding to Simulation 3 is seen to have the largest fractional free volume.

Figure 5 shows the bond anisotropy maps for the three carbon models considered here. The standard deviation of the bond anisotropy data and the $\alpha$ parameter for these simulations are listed in Table 6. The $\alpha$ parameter, which is a measure of the level of anisotropy, is only slightly different for these models indicating that the models have similar levels of anisotropy in terms of their bond directionality. Data for graphite, which has a highly anisotropic structure, are also shown in Table 6. Comparison of the $\alpha$ parameter of graphite with that of different carbon structures shows that the degree of anisotropy in the NPC models is almost an order of magnitude smaller than that in graphite.

Thus, the three models presented here are similar in terms of their chemical composition, local structural order (as quantified by the PDF), and level of anisotropy. However,

**Table 6. Standard Deviation of the Bond Anisotropy Data and the $\alpha$ Parameter for different Simulations**

| Simulation No. | Standard Deviation of Bond Anisotropy, $\sigma_\rho$ | $\alpha$ |
|---|---|---|
| 1 | 0.155 | 1.371 |
| 2 | 0.106 | 1.422 |
| 3 | 0.111 | 1.368 |
| Graphite | 0.0770 | 10.128 |

The simulation numbers correspond to those listed in Table 2. The data for graphite has also been added for reference since graphite is highly anisotropic.

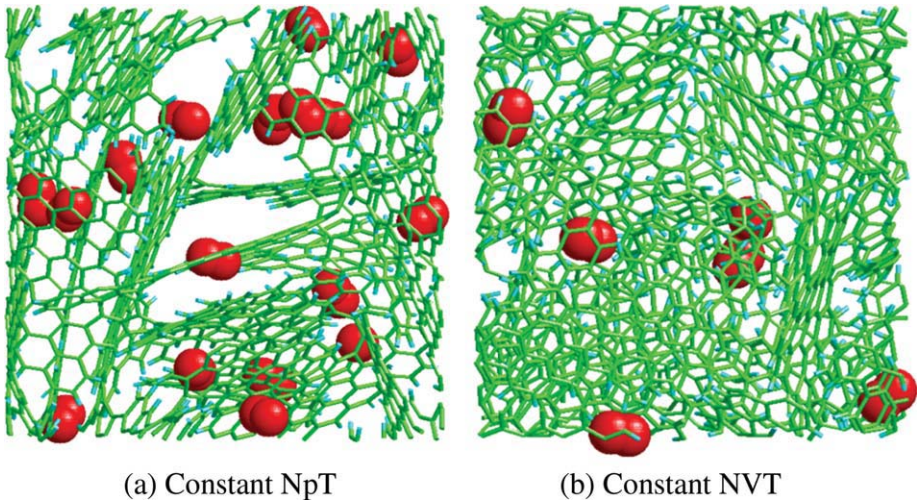


**Figure 6. Representative snapshots of nitrogen adsorbed at 298.15 K and 1 bar in (a) constant NpT model from Simulation 1 in Table 2 and (b) the corresponding constant NVT model.**

[Color figure can be viewed in the online issue, which is available at wileyonlinelibrary.com.]

the size and morphology of the cavities are different. This can be attributed to the nonequilibrium nature of the structures and the limited sample size. In comparison with the constant NVT carbon models, the constant NpT models have significantly larger cavities and void volume.

### *Nitrogen and oxygen adsorption in NPC models*

GCMC simulations are carried out to study the pure component adsorption of $N_2$ and $O_2$ in model NPC structures. Simulations are carried out with the total bulk pressure ranging from $10^{-2}$ to $10^{6}$ Pa. NPCs are amorphous, nonequilibrium structures and a single carbon model may not be sufficient to capture their adsorptive properties correctly. Hence, we use three models (corresponding to Simulations 1 through 3 from Table 2) generated at similar conditions of temperature and system size. These different models can be thought of as representations of different regions of a real NPC sample. To obtain a more realistic picture of gas adsorption in NPCs, the adsorption isotherms and isosteric heat of adsorption, $q_{st}$, of nitrogen and oxygen presented here are averaged over the three models. For the sake of comparison, adsorption properties for constant NVT models are also calculated (by averaging over three constant NVT models). Figure 6a shows snapshot of nitrogen adsorbed at 298.15 K and 1 bar in a constant NpT carbon model generated at conditions of

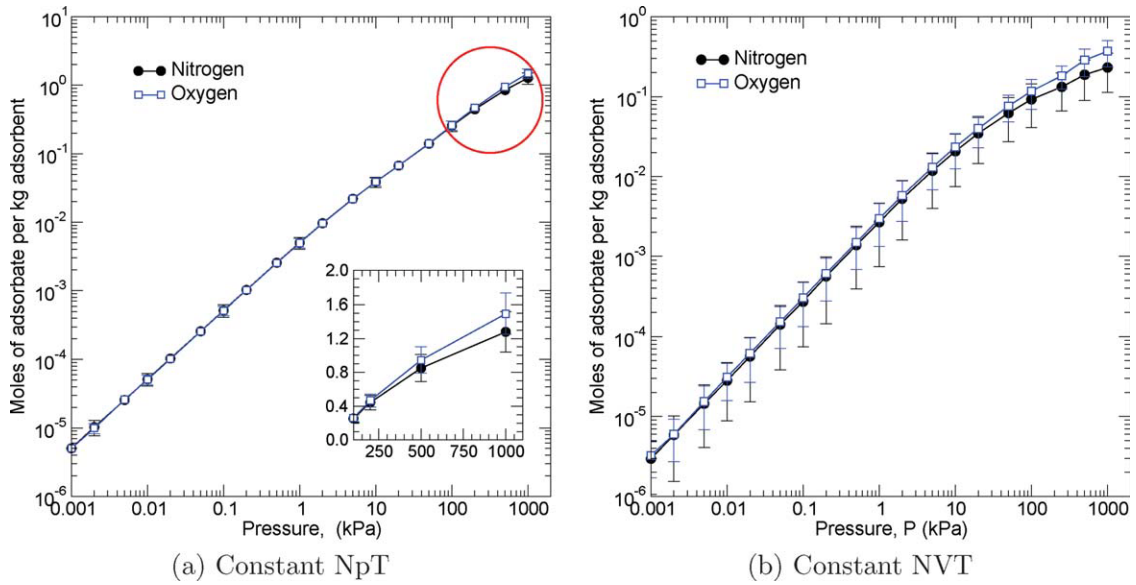


**Figure 7. Pure component adsorption isotherm of nitrogen and oxygen.**

(a) Adsorption isotherms of nitrogen and oxygen at 298.15 K obtained by averaging over NPC models from Simulations 1 through 3 (see Table 2). Inset shows a magnified view of the circled portion. (b) Average adsorption isotherms of nitrogen and oxygen at 298.15 K for constant NVT carbon models. [Color figure can be viewed in the online issue, which is available at wileyonlinelibrary.com.]

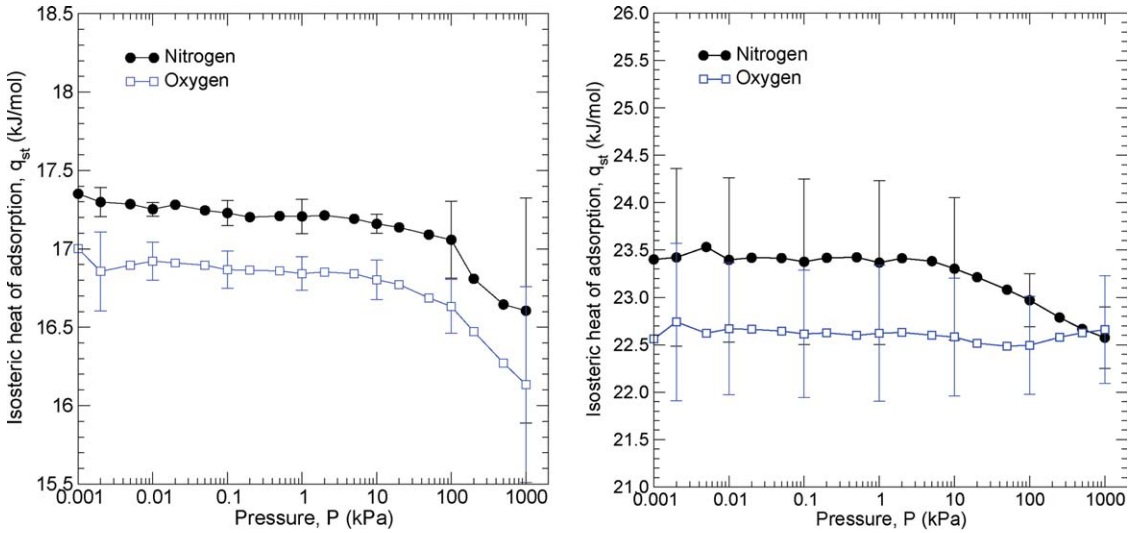


**Figure 8. The average is isosteric heats of adsorption of nitrogen and oxygen.**

(a) Isosteric heats of adsorption of nitrogen and oxygen at 298.15 K obtained by averaging over NPC models from Simulations 1 through 3 (see Table 2). (b) Average isosteric heats of adsorption of nitrogen and oxygen at 298.15 K for constant NVT carbon models. Only a few representative error bars are shown for clarity. [Color figure can be viewed in the online issue, which is available at wileyonlinelibrary.com.]

Simulation 1 in Table 2. Nitrogen adsorbed at the same conditions of temperature and pressure in the corresponding constant NVT model is shown in Figure 6b. The significantly higher amount adsorbed in the constant NpT carbon can be attributed to its larger free volume.

Figure 7a shows the pure component adsorption isotherms of nitrogen and oxygen at 298.15 K where the adsorbate-carbon interactions are represented by the Steele potential. Each isotherm in this figure is obtained by averaging the corresponding adsorption isotherms in NPC models obtained from Simulations 1–3 (see Table 2). Thus, for example, the adsorption isotherm of nitrogen at 298.15 K shown in Figure 7a is obtained by simulating the isotherms of nitrogen at 298.15 K in models from Simulations 1–3 and calculating the average of the three. At low-to-moderate pressures, the isotherms of nitrogen and oxygen are nearly identical. At high pressures (>100 kPa), the mean value of oxygen isotherm is observed to be slightly higher than that of nitrogen (see the inset of Figure 7a). However, a *t*-test performed on the data shows that the two isotherms are statistically indistinguishable. The average adsorption isotherms of nitrogen and oxygen in constant NVT carbon models are shown in Figure 7(b). The amounts of nitrogen and oxygen adsorbed are seen to be significantly lower than those for the constant NpT models.

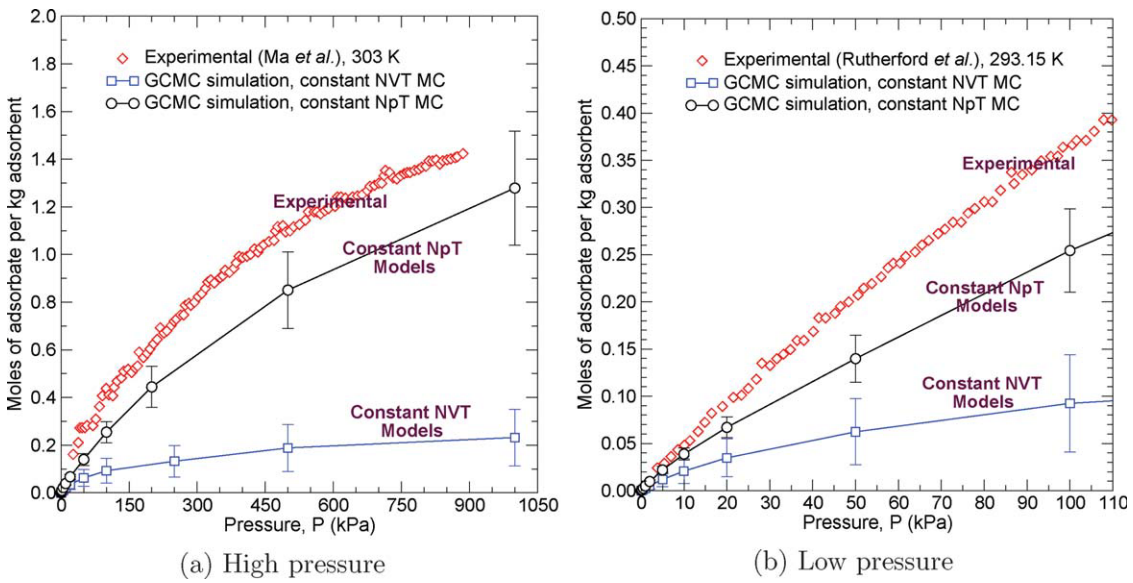


**Figure 9. Comparison of adsorption isotherm of nitrogen in experimental and model NPCs.**

The experimental data in (a) is from Ma et al.[25] and that in (b) is from Rutherford et al.[27] The constant NpT MC isotherms are obtained by averaging over models from Simulations 1 through 3 (see Table 2). The average isotherm for corresponding constant NVT models has also been shown. [Color figure can be viewed in the online issue, which is available at wileyonlinelibrary.com.]

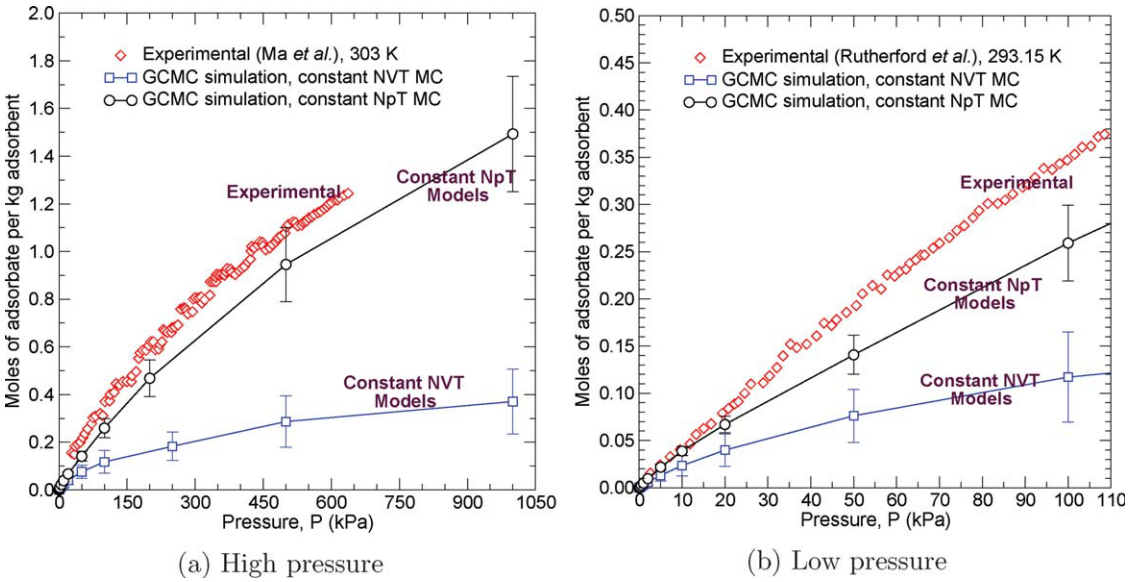


**Figure 10. Same as Figure 9 except that adsorption isotherms of oxygen are compared.**

The experimental data in (a) is from Ma et al.[25] and that in (b) is from Rutherford et al.[27] [Color figure can be viewed in the online issue, which is available at wileyonlinelibrary.com.]

Figure 8a shows the average isosteric heats of adsorption of nitrogen and oxygen in the constant NpT carbon models using Steele potential. Nitrogen is seen to have a slightly higher $q_{st}$ than oxygen. The difference however is not significant (<0.5 kJ/mol). In Figure 8b, the average isosteric heats of adsorption of nitrogen and oxygen in the constant NVT carbon models are shown. Although the mean $q_{st}$ values for the two gases differ by almost 1 kJ/mol at low-to-moderate pressures, the error bars are large and they overlap. The larger void volume in NPCs generated by constant NpT MC method leads to lower $q_{st}$ values than in NPCs generated by constant NVT MC method. This is evident on comparing Figures 8(a,b), where the $q_{st}$ values are 5–6 kJ/mol higher for NPCs generated by the constant NVT MC method. Experimental values of isosteric heats of adsorption in nanoporous carbons (Takeda, Bergbau-Forschung, etc.) range from 17 to 21 kJ/mol for nitrogen and 16.5 to 20 kJ/mol for oxygen.[27] In the case of constant NVT carbon models, the isosteric heats obtained from simulations (see Figure 8b) are somewhat higher than experimental isosteric heats of adsorption. On the other hand, isosteric heats of adsorption in carbon models generated from constant NpT MC method are generally within the range of experimental values (mentioned above). Therefore, the constant NpT carbon models provide a better representation of real NPCs than the constant NVT models.

In Figure 9, experimental adsorption isotherm of nitrogen is compared with the simulated isotherms. Figure 9a shows high pressure experimental data from Ma et al.[25] whereas Figure 9b shows low pressure experimental data from Rutherford et al.[27] The high pressure experimental data is for Takeda 5A carbons at 303 K, whereas the low pressure data is for Takeda 3A carbons at 293 K (both Takeda 3A and 5A are carbons molecular sieves). The simulated isotherms shown are all generated at 298.15 K. From Figures 9(a,b), it is evident that the average simulated isotherm obtained using NPCs generated by constant NpT MC method as the adsorbent is more representative of the experimental isotherms for both low and high pressures. On the other hand, the isotherm obtained using constant NVT carbons is much lower than the experimental isotherm. The larger free volume in constant NpT MC carbons results in higher adsorption capacity under similar conditions of temperature, pressure, and interaction potential. For oxygen (see Figure 10), the experimental adsorption isotherm is more closely resembled by isotherms obtained when NpT MC carbons are used as adsorbents. Note that the experimental data for oxygen was obtained from the same source as that for nitrogen. Isosteric heat values and Figures 9 and 10 lead us to conclude that carbon models generated by constant NpT MC method are a better representation of real nanoporous carbons than the models generated by constant NVT MC method as far as the adsorptive properties are concerned.

## Conclusions

The constant NpT MC algorithm produces carbon models that have larger cavities and higher free volumes than those generated by constant NVT method under similar simulation conditions. Some structures even show the presence of "holes" extending across the simulation box that would be suitable for allowing gas transport through the structure. NPC structures created (using constant NpT MC algorithm) from different starting structures do not differ appreciably in terms of their local structural order (as quantified by the PDF), chemical composition (quantified by the carbon-to-hydrogen ratio), and the fraction of different-sized carbon rings. Comparison with experiments show good agreement with the target (800°C) structure in terms of PDF and chemistry. However, the extended hole structure in the constant NpT MC simulations leads to densities that are somewhat lower than experimental NPC density. Apparently, the low formation pressure in the constant NpT simulations leads to opening of large, sample-spanning cavities that do not anneal or close during the course of the simulation.

The adsorption of gases in NPC models is studied using GCMC simulation. NPC models generated using constant NpT MC method exhibit higher adsorption and lower

isosteric heats for both adsorbates than those generated by constant NVT MC method. Isosteric heats of both gases lie within the experimental range for adsorption in constant NpT models. The constant NVT carbon models, on the other hand, exhibit higher $q_{st}$ values on an average than the experimental isosteric heats. The constant NpT MC models also show reasonably good semiquantitative agreement with experimental data for both adsorbates with respect to the adsorption isotherms. Thus, NPCs generated by constant NpT MC method are good representation of real NPCs in terms of the adsorptive properties.

## Acknowledgments

This work was supported by NSF Grant No. EEC-0085461. Useful discussions with Dr. Jan H. D. Boshoff about the MC simulations and with Dr. Michael A. Smith are gratefully acknowledged.

## Literature Cited

1. Franklin RE. Crystallite growth in graphitizing and non-graphitizing carbons. *Proc R Soc Lond Ser A Math Phys Sci*. 1951;209:196–218.
2. Rao MB, Sircar S. Performance and pore characterization of nanoporous carbon membranes for gas separation. *J Membr Sci*. 1996; 110:109–18.
3. Strano MS, Foley HC. Synthesis and characterization of heteropolyacid nanoporous carbon membranes. *Catal Lett*. 2001;74:177–184.
4. Shiflett MB, Foley HC. Ultrasonic deposition of high-selectivity nanoporous carbon membranes. *Science*. 1999;285:1902–1905.
5. Ruthven DM, Farooq S, Knaebel KS. *Pressure Swing Adsorption*. New York: VCH publishers Inc., 1993.
6. Smit B, Siepmann JI. Simulating the adsorption of alkanes in zeolites. *Science*. 1994;264:1118–1120.
7. Jiang J, Sandler S, Schenk M, Smit B. Adsorption and separation of linear and branched alkanes on carbon nanotube bundles from configurational-bias Monte Carlo simulation. *Phys Rev B*. 2005;72: 045447.
8. Heuchel M, Davies GM, Buss E, Seaton NA. Adsorption of carbon dioxide and methane and their mixtures on an activated carbon: simulation and experiment. *Langmuir*.1999;15:8695–8705.
9. Van Tassel PR, Ted Davis H, McCormick AV. Adsorption simulations of small molecules and their mixtures in a zeolite micropore. *Langmuir*. 1994;10:1257–1267.
10. Vlugt TJH, Krishna R, Smit B. Molecular simulations of adsorption isotherms for linear and branched alkanes and their mixtures in silicalite. *J Phys Chem B*. 1999;103:1102–1118.
11. Akten ED, Siriwardane R, Sholl DS. Monte Carlo simulation of single- and binary-component adsorption of $CO_2$, $N_2$, and $H_2$ in zeolite Na-4A. *Energy Fuels*. 2003;17:977–983.
12. Krishna R, van Baten JM. Using molecular simulations for screening of zeolites for separation of $CO_2/CH_4$ mixtures. *Chem Eng J*. 2007; 133:121–131.
13. Ghoufi A, Gaberova L, Rouquerol J, Vincent D, Llewellyn PL, Maurin G. Adsorption of $CO_2$, $CH_4$ and their binary mixture in Faujasite NaY: a combination of molecular simulations with gravimetry-manometry and microcalorimetry measurements. *Micropor Mesopor Mater*. 2009;119:117–128.
14. Arora G, Sandler SI. Air separation by single wall carbon nanotubes: thermodynamics and adsorptive selectivity. *J Chem Phys*. 2005;123: 044705.
15. Jiang SY, Zollweg JA, Gubbins KE. High-pressure adsorption of methane and ethane in activated carbon and carbon fibers. *J Phys Chem*. 1994;98:5709–5713.
16. Maddox MW, Sowers S, Gubbins KE. Molecular simulation of binary mixture adsorption in buckytubes and MCM-41. *Adsorption*. 1996;2:23–32.
17. Schumacher C, Gonzalez J, Pérez-Mendoza M, Wright PA, Seaton NA. Design of hybrid organic/inorganic adsorbents based on periodic mesoporous silica. *Ind Eng Chem Res*. 2006;45:5586–5597.
18. Ramsahye NA, Maurin G, Bourrelly S, Llewellyn PL, Devic T, Serre C, Loiseau T, Ferey G. Adsorption of $CO_2$ in metal organic frameworks of different metal centres: grand canonical Monte Carlo simulations compared to experiments. *Adsorption*. 2007;13:4617.
19. Walton KS, Snurr RQ. Applicability of the BET method for determining surface areas of microporous metal-organic frameworks. *J Am Chem Soc*. 2007;129:8552–8556.
20. Greathouse JA, Kinnibrugh TL, Allendorf MD. Adsorption and separation of noble gases by IRMOF-1: grand canonical Monte Carlo simulations. *Ind Eng Chem Res*. 2009;48:3425–3431.
21. Jiang J, Klauda JB, Sandler S. Monte Carlo simulation of $O_2$ and $N_2$ adsorption in nanoporous carbon ($C_{168}$ schwarzite). *Langmuir*. 2003; 19:3512–3518.
22. Jiang J, Klauda JB, Sandler S. Hierarchical modeling $O_2$ and $N_2$ adsorption in $C_{168}$ schwarzite: from quantum mechanics to molecular simulation. *J Phys Chem B*. 2004;108:9852–9860.
23. Vanderbilt D, Tersoff J. Negative-curvature fullerene analog of $C_{60}$. *Phys Rev Lett*. 1992;68:511–513.
24. Jiang J, Wagner NJ, Sandler SI. A Monte Carlo simulation study of the effect of carbon topology on nitrogen adsorption on graphite, a nanotube bundle, $C_{60}$ fullerite, $C_{168}$ schwarzite, and a nanoporous carbon. *Phys Chem Chem Phys*. 2004;6:4440–4444.
25. Ma YH, Sun W, Bhandarkar M, Wang J, Miller Gw. Adsorption and diffusion of nitrogen, oxygen, argon, and methane in molecular sieve carbon at elevated pressures. *Separ Technol*. 1991; 1:90–98.
26. Reid CR, O'koye IP, Thomas KM. Adsorption of gases on carbon molecular sieves used for air separation. Spherical adsorptives as probes for kinetic selectivity. *Langmuir*. 1998;14:2415–2425.
27. Rutherford SW, Coons JE. Adsorption equilibrium and transport kinetics for a range of probe gases in Takeda 3A carbon molecular sieve. *J Colloid Interface Sci*. 2005;284:432–439.
28. Darken LS. Diffusion, mobility and their interrelation through free energy in binary metallic systems. *Trans AIME*. 1948;175:184–201.
29. Kumar A, Lobo RF, Wagner NJ. Porous amorphous carbon models from periodic Gaussian chains of amorphous polymers. *Carbon*. 2005;43:3099–3111.
30. Allen MP, Tildesley DJ. *Computer Simulation of Liquids*. Oxford: Clarendon Press, 1987.
31. Frenkel D, Smit B. *Understanding Molecular Simulation*. London: Academic Press, 1996.
32. McDonald IR. NpT-ensemble Monte Carlo calculations for binary liquid mixtures. *Mol Phys*. 1972;23:41–58.
33. Eppinga R, Frenkel D. Monte Carlo study of the isotropic and nematic phases of infinitely thin hard platelets. *Mol Phys*. 984;52:1303–1334.
34. Molecular Simulations. *Cerius$^2$ Modeling Environment*. Sans Diego: Molecular Simulations, 1997.
35. Bojan MJ, Steele WA. Interactions of diatomic molecules with graphite. *Langmuir*. 1987;3:1123–1127.
36. Karavias F, Myers AL. Isosteric heats of multicomponent adsorption: thermodynamics and computer simulations. *Langmuir*. 1991;7:3118–3126.
37. Petkov V, DiFrancesco RG, Billinge SJL, Acharya M, Foley HC. Local structure of nanoporous carbons. *Philos Mag B*. 1999;79: 1519–1530.

*Manuscript received Apr. 19, 2010, and final revision received Jun. 25, 2010.*